01 Jan 2004

Optimizing Sequential Dual Tracer P.E.T. Studies Using a Combined 2D/3D Imaging Protocol

John W. Wilson
Missouri University of Science and Technology, jwilson@mst.edu

S. Borges-Neto

Timothy G. Turkington

James G. Colsher

et. al. For a complete list of authors, see https://scholarsmine.mst.edu/min_nuceng_facwork/1207

Recommended Citation

J. W. Wilson et al., "Optimizing Sequential Dual Tracer P.E.T. Studies Using a Combined 2D/3D Imaging Protocol," *Nuclear Science Symposium Conference Record, 2004 IEEE*, Institute of Electrical and Electronics Engineers (IEEE), Jan 2004.
The definitive version is available at https://doi.org/10.1109/NSSMIC.2004.1466452

Optimizing Sequential Dual Tracer P.E.T. Studies Using a Combined 2D/3D Imaging Protocol

John W. Wilson, Timothy G. Turkington, Member, IEEE, James G. Colsher, Member IEEE, Salvador Borges-Neto, Robert E. Reiman, R. Edward. Coleman

***Abstract*-- We have investigated a combined 2D/3D protocol for minimizing contamination in dual tracer P.E.T. studies in which the tracers are administered on a timescale that is short compared to the half-lives. We have performed a series of phantom studies on an Advance and a Discovery ST (GE Healthcare Technologies), using a torso phantom with cardiac insert (Data Spectrum Corporation) to simulate a combined FDG and NH_3 scan protocol for a patient with ischemia. The phantom was imaged in a series of alternating 2D/3D acquisitions as it decayed over 6 half-lives. By comparing 2D and 3D images, we have verified that 3D images are of comparable accuracy to 2D images, even with realistic out-of-field activity challenging the 3D scans. Based on scan and image statistical quality, we have recommended optimal doses for maximizing the image quality of both scans.**

I. Introduction

DUAL tracer P.E.T. studies suffer from contamination when the scans are performed on a timescale that is short compared to the half-lives. To minimize contamination in the resulting images, we have investigated a technique in which the first tracer is a low dose imaged in the higher-sensitivity 3D mode, and the second tracer is a much higher dose imaged in the lower-sensitivity 2D mode. The specific protocol we investigate is a combined FDG cardiac viability scan (initial low dose imaged in 3D) with an N-13 ammonia cardiac perfusion scan (high dose imaged in 2D) [1]. The N-13 Ammonia injection and scan follow immediately after the FDG scan, with the patient remaining on the scan table.

We have performed a series of phantom measurements, with the goal of optimizing the administered dose of both tracers to maximize the image quality of both images.

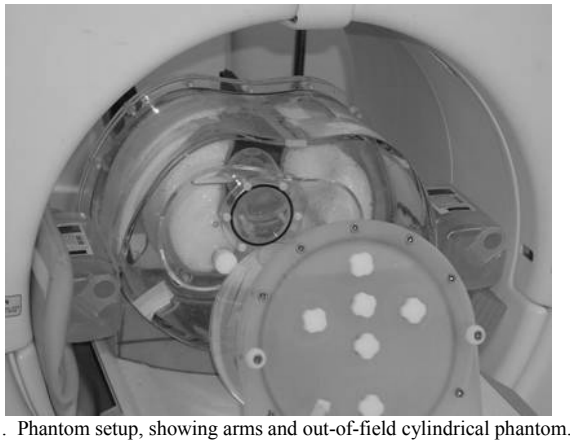

Fig. 1. Phantom setup, showing arms and out-of-field cylindrical phantom.

II. Methods

We have performed phantom measurements using a torso phantom with a cardiac insert (Data Spectrum Corp). A 5.4 ml fillable cardiac defect inside the 110 ml myocardium was used to simulate both a FDG hot defect (activity in defect, non-radioactive water in myocardium) and NH_3 cold defect (activity in myocardium, non-radioactive water in defect) scans for a patient with ischemia. For each scan type, realistic background and liver activity concentrations were used based on patient data. We use an estimate for the equivalent patient dose of 5 times the torso-phantom activity. The torso phantom was aligned in the scanner field of view, with one liter saline bottles (no activity) simulating arms. A separate 6 liter cylindrical phantom was placed near the phantom to provide out-of-field activity.

For each configuration (hot and cold defect) the torso phantom was imaged in a series of alternating 2D/3D 2 min acquisitions as it decayed from an initial activity of 560 MBq of F-18 (with an additional 560 MBq out-of-field activity in

Manuscript received November 1, 2004. This work was supported in part by GE Healthcare Technologies.

J. W. Wilson is with Department of Radiology of Duke University Medical Center, Durham, NC 27710 USA (telephone: 919-684-7978, e-mail: jwwilson@petsparc.mc.duke.edu).

T. G. Turkington is with Department of Radiology of Duke University Medical Center, Durham, NC 27710 USA (telephone: 919-684-7706, e-mail: timothy.turkington@duke.edu).

J. G. Colsher is with GE Healthcare Technologies, Milwaukee, WI (telephone: 919-401-8607, e-mail: james.colsher@med.ge.com).

S. Borges-Neto is with Department of Radiology of Duke University Medical Center, Durham, NC 27710 USA (telephone: 919-684-7857, e-mail: borge001@mc.duke.edu).

R. E. Reiman is with Duke University Medical Center Durham NC 27710 USA (telephone: 919-668-3186, e-mail: reima001@mc.duke.edu)

R. E. Coleman is with Department of Radiology of Duke University Medical Center, Durham, NC 27710 USA (telephone: 919-668-3186, e-mail: colem010@mc. duke.edu).

the cylindrical phantom) for 6.2 half-lives. Data were acquired on an Advance [2] and a Discovery ST [3] (GE Healthcare Technologies). All scans were reconstructed using filtered back projection due to its linearity.

From each image in the decay series, we acquired scan statistics (i.e., prompt and delayed counts), as well as region of interest (ROI) values for ~30 myocardium and ~30 background ROI's.

A. 2D and 3D Accuracy

To justify the combination of 2D and 3D scans in a single protocol, we first need to verify accuracy of the 3D images. To do this, we began by forming reduced-noise images by averaging five two-minute images. From these reduced-noise images, we extracted myocardial and background ROI's from both the 2D and 3D image sets. Taking the low-dose 2D images as the standard, we performed a region-by region comparison with the 3D images by dividing *each* 3D ROI value from a given slice by the a*verage* 2D ROI value from the same image slice. We expect these normalized ROI values to have a value near one for good 2D/3D agreement.

Because we are proposing to use a high dose for the 2D scan, we also need to verify that scanner performance in 2D does not degrade at high activity levels. To do this, we compared the average value of 30 2D myocardial ROI's as a function of activity, to a linear fit.

B. Evaluating Scan and Image Statistical Quality.

Using the scan statistics (prompt and delayed counts) we calculated an estimate of statistical quality for both the FDG-like scan and the contaminated NH_3 scan as a function of activity.

In the clinical protocol, the FDG scan is completed before the NH_3 is administered, and therfore it is uncontaminated. We can therefore model it with the hot defect scan data alone. We used the true and prompt counts from the hot defect scans to derive noise equivalent count rate (NEC) [4] curves as a function of activity.

To calculate statistical quality for an NH_3 scan contaminated with a small amount of residual FDG, we must combine data from the cold defect scan and the hot defect scan. For the case, in which the 3D FDG scan has been subtracted from the 2D NH_3 scan, the true counts that contribute to the signal come only from the cold defect scan, whereas the true and the prompt counts from both cold and hot defect scans contribute noise. Knowing this, we can derive an NEC-like estimate of contaminated scan statistical quality Q_{csub} as

$$Q_{csub} = \frac{(T_{cold})^2}{(P_{cold} + 2P_{hot} + 2T_{hot})}, \quad (1)$$

where T and P are the true and prompt counts from the hot and cold defect scans, and the factors of two in the denominator account for the additional noise added when subtracting the FDG image from the contaminated NH_3 image. If the FDG image is not subtracted from the contaminated NH_3 image, we do not have the additional noise introduced by the subtraction. However, the true counts in the FDG scan reduce the contrast in the contaminated image. For this case we use,

$$Q_c = \frac{(T_{cold} - T_{hot})^2}{(P_{cold} + P_{hot} + T_{hot})}. \quad (2)$$

For all cases we considered, we found that the improvement in contrast outweighed the increased noise. The rest of this paper will focus on this case.

To calculate image signal to noise ratio (SNR) for the FDG scan, we take the signal to be the difference between the average of the 30 hot myocardial ROI's and the average value of the background ROI's, and the noise to be the standard deviation of the background ROI's.

For the contaminated NH_3 image, we again must combine data from the hot and cold defect scans. For the case where the FDG image is subtracted from the NH_3 image, we use

$$SNR_{csub} = \frac{S_{cold}}{\sqrt{\sigma_{cold}^2 + 2\sigma_{hot}^2}} \quad (3)$$

Where S_{cold} is the difference between the average myocardial ROI value and the background, and σ_{cold} and σ_{hot} are the standard deviations of the cold and hot defect background ROI's respectively.

III. Results

A. 2D and 3D Accuracy

Figures 2 and 3 show results for the comparison of 2D and 3D accuracy. In fig. 2, we show a representative reduced-noise 2D and 3D image, and the subtracted image. Profiles through the images confirm that regional differences are small compared to image noise.

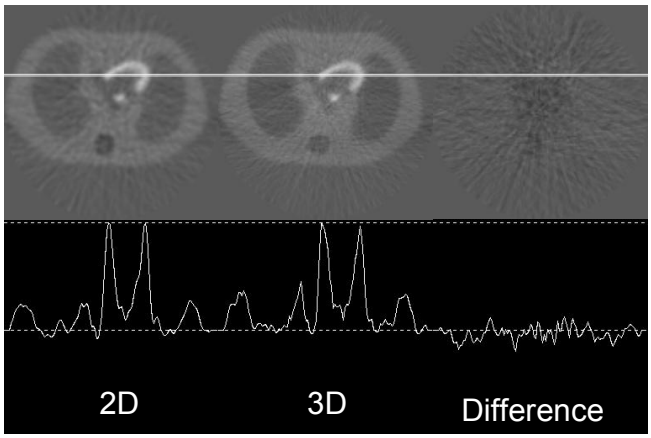

Fig. 2. Low-noise 2D and 3D images, and their difference for the Discovery ST.

Fig. 3 shows the ratio of several 3D myocardial ROI's and one 3D background ROI, all from the same randomly chosen image slice, to the average 2D ROI value from the same slice. The close agreement with the average 2D value, and the relatively small deviation in the individual 3D ROI values over

the chosen image slice validates the use of 3D for low activity levels.

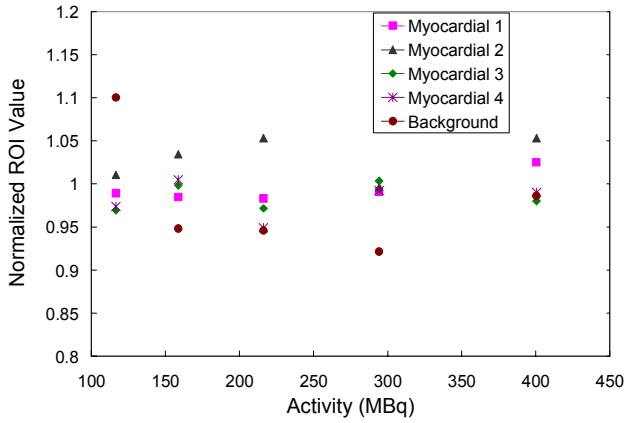

Fig. 3. ROI values for four 3D myocardial ROI's and one background ROI, normalized to the average 2D ROI value. (Discovery ST)

In Fig. 4, we compare the average 2D myocardial ROI value as a function of activity to a linear fit. That the 2D ROI values remain linear with activity up to at least 2500 MBq validates the use of a large 2D dose.

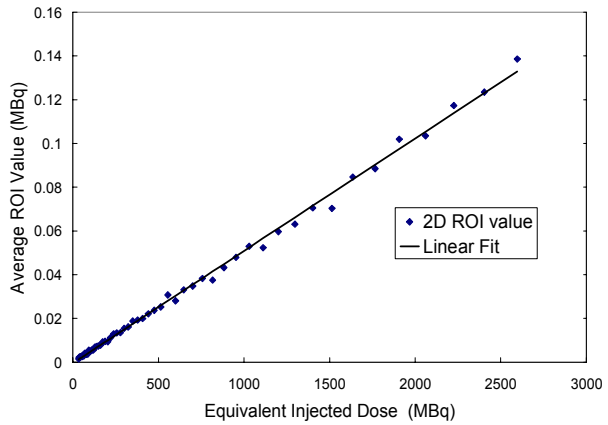

Fig. 4. Average 2D ROI value as a function of activity, compared with a linear fit.

B. *Evaluating Scan Statistical Quality.*

Figures 5 and 6 show scan statistical quality for the FDG-like hot defect and the contaminated NH_3 cold defect scans for the Discovery ST. For the NH_3 scan, we show curves for several values of FDG dose. The top-most curve represents the limit of no FDG contamination, and is equivalent to the 2D NEC. We see that increasing FDG dose decreases scan statistical quality, as expected.

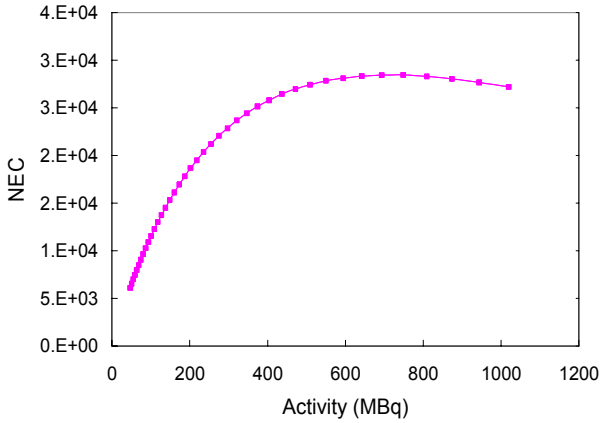

Fig. 5. 3D FDG Hot Defect NEC vs. Activity for the Discovery ST.

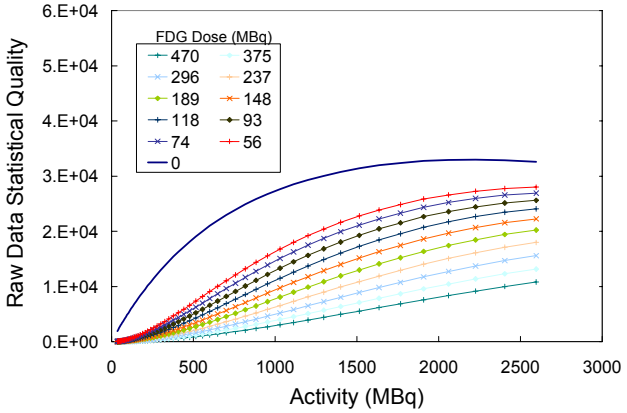

Fig. 6. Contaminated NH_3 scan statistical Quality vs. Activity for the Discovery ST.

Figures 7 and 8 show image SNR for the Discovery ST. We find that, although increasing FDG dose decreases the quality of the contaminated NH_3 scan, there is a point of diminishing returns, beyond which there is little further gain in SNR, even with large decreases in FDG dose.

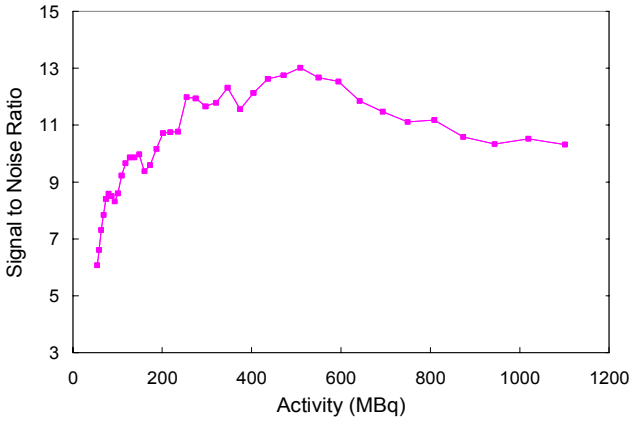

Fig. 7. Image Signal to Noise vs. equivalent patient activity for the DST hot defect scan

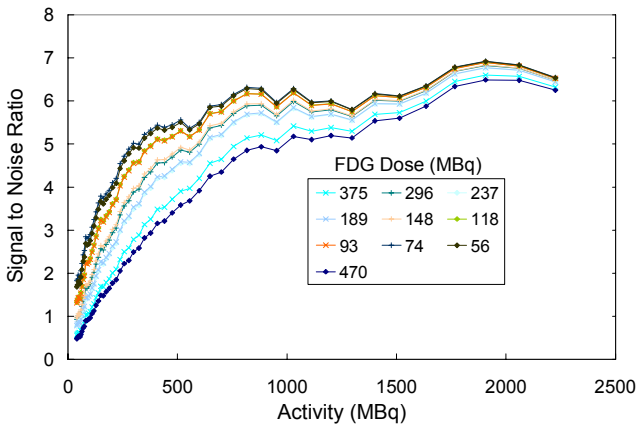

Fig. 8. Image Signal to Noise vs. equivalent patient activity for the contaminated DST cold defect scan.

This point corresponds to an FDG dose of ~ 300 MBq (Discovery ST) and ~ 200 MBq (Advance). For both scanners, the peak SNR occurs at a dose of ~ 1850 MBq of NH_3.

IV. Conclusions

We have used a series of phantom studies to investigate a combined 2D/3D imaging protocol designed to maximize image quality in dual tracer PET studies. We have verified that the 3D images are of comparable accuracy to the 2D images, even though we added significant out-of-field activity, and that scanner performance remains linear for large 2D doses. By combining data from hot and cold defect scans, we have been able to calculate the statistical scan quality and SNR for both the FDG-like scan and the contaminated NH_3 scan. Based on these calculations, we have made specific dose recommendations for optimizing the image quality of both scans. At these doses, the total whole body radiation dose [5] from both injections is equivalent to that of a 440 MBq FDG injection (Discovery ST) and a 330 MBq FDG injection (Advance).

V. Acknowledgement

We thank Mary Hawk, DeAndre Starnes and Jackie Ison for assistance with phantom studies. We also thank Sean Murphy, Amar Das and Michael Daley for radiotracer production support.

VI. References

[1] T. Tsuchida, N. Sadato, Y. Yonekura, K. Sugimoto, A. Nakano, J. D. Lee, N. Takahashi, A. Waki, Y. Ishii, H. Itoh. "Myocardial FDG-PET examination during fasting and glucose loading states by means of a one-day protocol" Ann Nucl Med. 2001 Oct; 15(5):433-8.

[2] T. R. DeGrado, T. G. Turkington, J. J. Williams, C. W. Stearns, J. M. Hoffman, R. E. Coleman. "Performance characteristics of a whole-body PET scanner". J Nucl Med. 1994;35:1398–1406.

[3] A. O. Mawlawi, D. A. Podoloff, S Kohlmyer, J. J. Williams, C. W. Stearns, R. F. Culp, and H. Macapinlac, "Performance characteristics of a newly developed PET/CT Scanner using NEMA standards in 2D and 3D Modes," J Nucl Med, vol. 45, no. 10, 1734-1742.

[4] S. C. Strother, M. E. Casey, E. J. Hoffman. "Measuring PET scanner sensitivity: relating countrates to image signal-to-noise ratios using noise equivalent counts," IEEE Tr. Nuc. Sci., vol 7 no.2 Pp. 783-788 April 1990 169.

[5] A. H. Lockwood., J. M. McDonald, R. E. Reiman, A. S. Gelbard, J. S. Laughlin, T. E. Duffy, and F. Plum. "The dynamics of ammonia metabolism in man. Effects of liver disease and hyperammonemia." J. Clin. Invest. 63: 449-460, 1979